Changes of summer cloud water content in China from ERA-Interim reanalysis

Qinglong You [1,2]*, Juju Liu[2], Nick Pepin[3]

1. Department of Atmospheric and Oceanic Sciences & Institute of Atmospheric Sciences, Fudan University, 200438, Shanghai, China;

2. Key Laboratory of Meteorological Disaster, Ministry of Education (KLME), Nanjing University of Information Science and Technology (NUIST), Nanjing, 210044, China;

3. Department of Geography, University of Portsmouth, U.K.

* Corresponding author E-mail address: yqingl@126.com

Abstract:

Cloud plays an important role in regulating radiation and energy exchange, and the hydrological cycle. In this study, the variability of summer vertical integral cloud water content (VCWC) (sum of cloud liquid water content and cloud ice water content) from ERA-Interim reanalysis is investigated over China from 1979-2016. We divide the country into regions dominated by monsoonal and non-monsoonal influences, and the Tibetan Plateau. Relationships between summer VCWC and surface mean temperature, precipitation and precipitable water (PW) are investigated by singular value decomposition. Summer VCWC decreases from southeast to northwest with the largest values in the southwestern China. Summer VCWC has increased in the non-monsoon and Tibetan Plateau sub-regions with rates of 1.04 and 3.39 g/m^2/decade respectively, which corresponds to an increase of PW, precipitation and surface mean temperature. Summer VCWC has decreased by -2.71 g/m^2/decade in the monsoon sub-region, related to decreased precipitation and PW as well as increased surface mean temperature. Temperature rises (decreases) will strengthen (weaken) the atmospheric circulation in favor of increased (decreased) summer VCWC in the non-monsoon/Tibetan Plateau sub-region, but weaken (strengthen) the climate systems in the monsoon sub-region. This explains the contrasting correlations between temperature and summer VCWC in the different regions, suggesting summer VCWC in China is moderated by atmospheric circulation through combined influences of surface mean temperature and PW.

Key words: China; cloud water content; trend;

1 Introduction

Cloud properties which include cloud water content (CWC) (sum of cloud liquid water content (CLWC) and cloud ice water content (CIWC)), cloud water path, cloud effective radius, cloud height and cloud thickness, play an important role in regulating both the energy and water budgets at the Earth's surface. In doing so, they also regulate the response of the atmospheric circulation to climate change [*Gultepe and Isaac*, 1997; *Ntwali et al.*, 2017; *Yang and Wang*, 2012]. In climate models, clouds provide a link between the hydrological and atmospheric systems and thus have an important impact on the climate system, and are probably the largest uncertainty in understanding of climate change [*Bony et al.*, 2015; *IPCC*, 2013; *Norris et al.*, 2016]. The Intergovernmental Panel on Climate Change (IPCC) Fifth Assessment Report (AR5) reveals that the mean global surface air temperature has warmed by 0.85 [0.65 to 1.06]°C over the period 1880 to 2012 [IPCC, 2013]. Such warming should moderate the physical processes and attendant characteristics of clouds.

Temperature increases in China since the 1950s are shown to be more rapid than the global mean [*Bannister et al.*, 2017; *Ding et al.*, 2007; *H J Wang et al.*, 2012]. However, it is unclear how this temperature increase has influenced cloud properties over the same period. The occurrence and development of clouds and resultant precipitation are complex and remain sufficient obstacles to successful weather and climate prediction. This is because there are numerous cloud-radiation feedback processes which have to be combined in a climate model [*Gultepe and Isaac*, 1997; *Ntwali et al.*, 2017; *Yang*

65 *and Wang*, 2012]. CWC is critical for numerical weather prediction and climate
66 projections [*Yang and Wang*, 2012], and some studies have analyzed characteristics of
67 CWC in China using data from the ISCCP (International Satellite Cloud Climatology
68 Project), Cloudsat satellite and ERA-Interim datasets [*J Li et al.*, 2017a; *C Wu and*
69 *Chou*, 2013; *Zhai and Eskridge*, 1997]. These studies have shown that there is a clear
70 seasonal change in both the amount and spatial distribution of CWC in China, and
71 summer CWC is strongly influenced by the Asian summer monsoon, the topography of
72 Tibetan Plateau, and variation in exposure to the mid-latitude westerly flow [*X Li et al.*,
73 2011; *Yang and Wang*, 2012; *Zhou and Yu*, 2005].

74 However, there is limited studies on changes in summer CWC in China. Furthermore,
75 understanding the physical and dynamical structures of clouds and therefore successful
76 incorporation of cloud feedbacks into model simulations, is strongly dependent on how
77 accurate CWC can be modelled in the atmosphere. In this study, the patterns and causes
78 of temporal and spatial variation in summer CWC in China are studied which will
79 provide essential understanding for future model development over the region.

80 **2 Dataset and method**

81 The ERA-Interim reanalysis data released by European Centre for Medium-Range
82 Weather Forecasts (ECMWF) [*Dee et al.*, 2011] is selected in this study. ERA-Interim
83 is the most comprehensive set of assimilation satellite observation data in reanalysis
84 data. It is an updated data set of ERA-15 and ERA40. Its cloud water content data is
85 the forecast variables based on observation data and forecast mode [*Dee et al.*, 2011].

ERA-Interim is generated using the ECMWF Integrated Forecasting System (IFS) Cy31r2 model and four-dimensional variational data assimilation (4D-Var). The horizontal resolution is increased to T255 with 37 vertical levels from 1000 hPa to 1 hPa (http://data.ecmwf.int/data) [*Dee and Uppala*, 2009; *Dee et al.*, 2011]. The period January 1979 to December 2016 is selected and June-August is defined as summer.

The climatic elements including specific humidity (q), CWC, CLWC and CIWC are obtained from ERA-Interim reanalysis. In addition, observations of surface mean temperature (2m) and precipitation in China for 1979–2015 are available as a high-quality daily gridded dataset with 0.5°×0.5° resolution interpolated from 2400 stations [*J Wu and Gao*, 2013; *Xu et al.*, 2009]. This was obtained from National Meteorological Information Center, China Meteorological Administration (http://data.cma.cn.).

To calculate the available water in the whole atmospheric column, the precipitable water (PW), the vertical integral of CLWC (VCLWC) and CIWC (VCIWC) are calculated as the vertically integrated horizontal transport between 1000 hPa and 300 hPa using atmospheric reanalysis data. The vertical integral of CWC (VCWC) is the sum of VCLWC and VCIWC.

Methods for objectively analyzing the relationship between time and space change of two fields are MEOF (Multivariable Empirical Orthogonal Function), PCA (Single-Filed-based PCA), CCA (Canonical Correlation Analysis), and SVD (singular value decomposition) [*H B Wu and Wu*, 2005]. Among them, SVD is the easiest to implement and explain. The SVD method is one of the most widely-used multivariate statistical

techniques used in atmospheric science to determine the correlation patterns of two independent fields [*Lanzante*, 1984; *Wallace et al.*, 1992].

The SVD method yields two singular vectors which define two sets of spatial patterns relevant to two input fields, and the expansion coefficients are computed from the two singular vectors separately. The singular values provide a measure of the fraction of the squared correlation accounted for by the corresponding singular vector, in the same manner as the eigenvalues of a correlation matrix provide a measure of the percentage of variance explained by eigen modes [*Lanzante*, 1984; *Shen and Lau*, 1995; *Wallace et al.*, 1992]. To compare the results with maps of correlation coefficients, the singular vector matrices are scaled to one, equivalent to the temporal correlation coefficient between the expansion coefficient of the corresponding mode and the field variable at that same grid point [*Wallace et al.*, 1992].

To study the relationships between the two field structures, the SVD method is applied to the correlations between precipitation, temperature, PW and VCWC in China. To identify statistically significant patterns from random noise, a Monte Carlo technique has been applied to test the significance of the SVD results [*Overland and Preisendorfer*, 1982].

Three sub-regions in China are defined by topography and geographical location (Figure 1) including 1) non-monsoon sub-region, 2) Tibetan Plateau sub-region and 3) monsoon sub-region, respectively. The demarcation line between the monsoon and non-monsoon climate zones (Daxinganling - Yinshan Mountains - Helan Mountain -

Wushaoling - Bayan Hara - Tanggula - Gangdisi) and the geographical boundary of the Tibetan Plateau define the sub-regions [*Ding et al.*, 2007; *Liu et al.*, 2004; *H J Wang et al.*, 2012; *S W Wang and Gong*, 2000; *Y Q Wang and Zhou*, 2005] .

3 Results

3.1 Climatological distribution

Figure 2 shows the climatological distribution of VCLWC, VCIWC, VCWC, PW, surface mean temperature and precipitation in China in summer (JJA) during 1979-2016. VCLWC decreases from the south and south-east to the north-west (Figure 2a), and VCIWC tends to be higher in southern regions, peaking in the western Sichuan basin (Figure 2b). The spatial distribution of VCWC is broadly similar to VCLWC, with largest values (> 0.25 kg/m^2) in the south-west and smallest values (<0.05 kg/m^2) in the north-west (Figure 2c). PW is most concentrated in the southern and eastern parts of China, rather than Sichuan, and the maximum is slightly further east than VCLWC and VCIWC (Figure 2d). The distribution of surface mean temperature is strongly negatively correlated with elevation, as expected (Figure 2e). Precipitation decreases from south-east to north-west and has a broadly similar pattern to PW (Figure 2f).

Figure 3 shows pressure-latitude cross sections of CLWC, CIWC, and CWC for the three sub-regions. In the monsoon sub-region (top row), CLWC is concentrated around 22-36°N, 925~450hPa, -10~25℃ (Figure 3a), and the highest CIWC occurs between 27 and 40°N (Figure 3b). CWC on the other hand is concentrated south of 36°N and

between 850~400hPa and -15-20℃. Values above 0.03g/kg are recorded at both 850 and 500hPa (Figure 3c). In the non-monsoon sub-region (second row), CLWC is much lower and mainly located at the domain of 800~400hPa, 15~-10℃ (Figure 3d). CIWC is negligible over most of the domain (Figure 3e). CWC relates to topography, and surprisingly mountainous areas around 38°N in the south of the region show large values reaching over 0.02g/kg around 600-300 hPa, -40~5 ℃ (Figure 3f). CWC therefore increases from north to south. In the Tibetan Plateau sub-region (bottom row), CLWC shows a distinct peak south of 31°N and below 450hPa. Large values of >0.04 g/kg create a plume of moist air which extends up from the surface to 500 hPa and also extends slightly further north at around the 500 hPa level (Figure 3g). The maximum CIWC on the other hand is further north around 34-36°N and at higher elevations (Figure 3h). CWC overall is dominated by CLWC so shows a similar distribution to the liquid component (Figure 3i).

In summary, VCWC is lowest in the non-monsoon sub-region (middle row) with slightly higher values in the mountainous areas of Xinjiang. VCWC in the Tibetan Plateau sub-region is extremely high particularly in the south. These patterns are broadly consistent with the distribution of precipitation and PW in these regions. VCWC in the monsoon sub-region shows a strong decreasing gradient from south to north but is nowhere near as high as in the southern parts of the Tibetan plateau sub-region.

3.2 Time series and trends

Figure 4 and Figure 5 represent time series and spatial trends of VCLWC, VCIWC, VCWC, PW, mean temperature and precipitation in the three regions in summer between 1979 and 2016. Table 1 summarizes the magnitude of some of these trends. In the monsoon sub-region (top graphs on Figure 4), both VCLWC and VCIWC decrease over most of the period, but there was a temporary increase in the 1990s. Both show similar inter-annual variability, with high correlation between them. Thus VCWC as a whole shows a similar decreasing trend. During the same period, PW on the other hand shows relatively little change, while temperature has increased and precipitation has shown no overall decrease. Therefore although precipitation shows broad similarities to VCWC and its components, it is not shown such a strong decrease as might be expected from the decline in VCLWC.

In the non-monsoon sub-region (middle graphs on Figure 4), VCLWC, VCIWC and VCWC show similar inter-annual variation, and overall there appears to be an increasing trend, although this is strongly influenced by the most recent years. PW has also increased, and the value for 2016 is exceptional. The rapid warming of surface mean temperature is clear, and the general increase in precipitation appears to be significantly correlated with VCLWC, VCIWC and VCWC.

In the Tibetan Plateau sub-region (bottom graphs on Figure 4), VCLWC, VCIWC and VCWC trends in general show an increase, but there has been a levelling off after the mid-1990s, similar to the non-monsoon sub-region. VCIWC has even decreased since

189 the turn of the century. PW however shows a strong increasing trend, as does the surface
190 air temperature.

191 Maps of spatial trends (Figure 5) show this in more detail. VCLWC, VCIWC and
192 VCWC show broadly similar trend patterns, with the strongest positive trends over the
193 whole period in western parts of China (west of 105°E). The heart of northern and
194 eastern China in the monsoon sub-region shows a decrease, particularly marked for
195 VCIWC. PW shows most increase in western China and some coastal provinces
196 whereas much of central China shows a negative trend. Surface mean temperature has
197 shown pronounced warming everywhere, but especially at high elevations and latitudes.
198 The most significant positive trends for precipitation occur in western China, which is
199 similar to VCWC.

200 Table 1 lists trend values for the three sub-regions as a whole, and significant contrasts
201 between regions are demonstrated. VCWC has increased most strongly in the Tibetan
202 plateau region, along with PW. However trends in precipitation are insignificant. In
203 summary, the three regions show some differences in trends, with the increases in
204 VCWC being most systematic and widespread in the non-monsoon and Tibetan plateau
205 sub-regions. VCWC shows significant inter-annual variation in the three sub-regions
206 with the strongest long-term increase in parts of the non-monsoon and Tibetan Plateau
207 sub-regions.

208 **3.3 SVD analysis**

209 Figure 6 shows the heterogeneous correlation between VCWC and PW (top
210 row)/surface mean temperature (middle row)/precipitation (bottom row) and the time
211 coefficient of the first mode of SVD for each respectively. Table 2 summarizes the
212 correlation coefficients between VCWC, VCLWC, VCIWC, precipitation, PW and
213 surface mean temperature in the three sub-regions during 1979-2016. In this way the
214 various contributing factors towards variance in VCWC can be examined.

215 The first SVD mode for PW/VCWC represents 13% of the total variance, and the
216 correlation coefficient between the expansion coefficients of the first SVD is 0.87,
217 which passes Monte-Carlo significance at $p<0.05$ (Figure 6 a, b, c). For PW patterns,
218 positive correlations occur for most of China, especially in the non-monsoon and
219 Tibetan Plateau sub-regions. Some negative correlations are demonstrated in eastern
220 China. This suggests that an increase (decrease) of PW in the non-monsoon and Tibetan
221 Plateau sub-regions corresponds to a simultaneous increase (decrease) of VCWC in
222 western China and decrease (increase) in eastern China.

223 The first SVD mode for surface mean temperature/VCWC represents 33.2% of the total
224 variance, and the correlation coefficient between the expansion coefficients of the first
225 SVD is 0.85 ($p<0.05$) (Figure 6 d, e, f). Mean temperature shows positive correlations
226 for the whole of China. VCWC shows positive correlations west of 105°E (except in
227 the Xinjiang basin and central Yunnan basin), Jiangnan and South China, but negative
228 correlations in most of eastern China. In most areas therefore an increase (decrease) of
229 surface mean temperature in China corresponds to an increase (decrease) of VCWC in

western China and the opposite in eastern China.

The first SVD mode for precipitation/VCWC represents 10.4% of the total variance, and the correlation coefficient between the expansion coefficients of the first SVD is 0.92 ($p<0.05$) (Figure 6 g, h, i). The precipitation shows positive correlations in northeast China and negative correlations in the northwest of the Tibetan Plateau and in southeast China. VCWC shows similar correlations patterns as precipitation. This suggests that the two variables are very strongly coupled. An increase (decrease) of precipitation in northeast China and decrease (increase) of precipitation in the north-west of Tibetan Plateau corresponds to an increase (decrease) of VCWC.

3.4 Atmospheric circulation analysis

To demonstrate how the atmospheric circulation interacts with VCWC in the monsoon (Figure 7), non-monsoon (Figure 8) and Tibetan Plateau (Figure 9) sub-regions respectively, atmospheric composite analyses of wind fields and wind speeds contrasting between strongly positive and negative VCWC years have been performed.

For the monsoon sub-region (box on Figure 7), low pressure in the Mongolian region at 700 hPa intensifies water vapor convergence and encourages strong upward motion which is beneficial to the formation of VCWC over the monsoon sub-region (Figure 7a). Strong southwesterly airflow covers most of southern China to the east of the Tibetan Plateau and moisture is also pumped northwards around a high pressure ridge over Taiwan (Figure 7c). Both the Mongolian cyclone and the eastern Tibetan Plateau

250 trough contribute to an increase of VCWC.

251 The atmospheric composite patterns of wind field and wind speed between the strongly
252 positive and negative surface mean temperature years at both 700 hPa and 500 hPa are
253 completely opposite to those for VCWC (Figure 7b,d). Warmth (cold) in the monsoon
254 sub-region weakens (strengthens) the southwest summer monsoon, the eastern Plateau
255 trough and the Mongolian cyclone, and therefore reduces (increases) the ascending
256 motion of water vapor, resulting in reduced (increased) VCWC. This explains why the
257 correlation between VCWC and surface mean temperature is strongly negative in the
258 monsoon sub-region (R=-0.51, Table 2). More warming in the north of monsoon sub-
259 region decreases the latitudinal temperature gradient and therefore the pressure gradient
260 and weakens the East Asian summer monsoon. This in turn limits water vapor
261 transportation to the monsoon sub-region. The reduction of VCWC will increase the
262 surface shortwave solar radiation flux and further increase the surface mean
263 temperature, forming a negative feedback mechanism between VCWC and surface
264 mean temperature in the monsoon sub-region.

265 In the non-monsoon sub-region (Figure 8), the composite analysis of wind field and
266 wind speed at 700hPa and 500hPa indicates four possible water vapor channels
267 contributing to VCWC. These are 1) southwesterly airflow around a cyclone over the
268 Caspian Sea, 2) airflow originating from polar latitudes near Lake Baikal and arriving
269 from the south-east after diverging from the Mongolian anti-cyclone, 3) southerly
270 airflow to the east of a cyclone over the western Arabian Sea, and 4) southeasterly

airflow originating from the Bay of Bengal arriving after traversing the Tibetan Plateau. The channels from the Mongolian anticyclone and the Bay of Bengal are strengthened by southeasterly airflow from South China Sea and the northwest Pacific Ocean. The dominant flow in the non-monsoon sub-region (box on Figure 8) appears to come from the high-latitude climate system, suggesting that meridional water vapor transport is critical to this region. It appears that the patterns for increased surface mean temperature are very similar to those for increased VCWC in this region, which implies that surface warming and increased VCWC are coupled together. Warming will increase both evaporation and saturation vapor pressure, which will cause an increase in PW. Moreover, the surface warming will tend to destabilize the atmosphere, and further promote VCWC increase. VCWC increase will help the formation of precipitation and prevent longwave radiation loss which could result in further warming.

In the Tibetan Plateau sub-region (Figure 9) at 500 hPa, the composite shows that three water vapor channels contribute to high VCWC: 1) southwesterly airflow to the east of a cyclone over Eastern Iran, 2) southwesterly airflow from Indian Ocean originating from the Bay of Bengal and ascending onto the plateau, and 3) southeasterly airflow from North-western Pacific and Southern China. It can be noted that these airflows mainly come from the western and southern inflow. A marked convergence zone between the southwesterly and southeasterly flows occurs near 32°N over the central Tibetan Plateau, which is conducive to ascending motion and an increase in VCWC. Composite patterns of the wind field at 500 hPa between strongly positive and negative surface mean temperature show that surface warming will strengthen both water vapor

293 channels and the wind shear over the plateau.

294 At 200 hPa, high pressure located over the Tibetan Plateau encourages upper level
295 divergence, and therefore uplift and strong convective activity and high VCWC. The
296 composite pattern of the wind field at 200 hPa suggests that significant warming will
297 strengthen this upper level (South Asia) high. More warming in the Tibetan Plateau sub-
298 region in comparison with regions to its south will increase the reversed meridional
299 temperature gradient and strengthen the South Asian summer monsoon, resulting in
300 more water vapor transport to the Tibetan Plateau sub-region. At the same time,
301 warming in the lower troposphere will increase instability, strengthen upwards motion,
302 enhance the upper-level South Asia high, promote convection, and further increase
303 VCWC and precipitation. In turn, any VCWC increase will weaken longwave radiation
304 loss which will result in temperature rise, especially at high elevations.

305

306 **4 Summary and Conclusions**

307 Based on reanalysis data sets (ERA-Interim) and station observations (precipitation and
308 temperature), this study investigates patterns of summer CWC and its relationships with
309 atmospheric circulation in three different regions of China during 1979-2016. Overall,
310 both VCLWC and VCWC decrease from southeast to northwest, but the largest values
311 are reported in the southwest. VCIWC has large values in the central regions of China
312 with the largest value in western Sichuan. During the studied period, VCWC has

313 increased in the non-monsoon and Tibetan Plateau sub-regions by 1.04 and 3.39
314 g/m^2/decade respectively, which corresponds with simultaneous increases of PW,
315 precipitation and surface mean temperature. In contrast, VCWC has decreased by -2.71
316 g/m^2/decade in the monsoon sub-region, related to a decrease in precipitation and PW
317 alongside the increase in surface mean temperature.

318 VCWC is moderated by the atmospheric circulation through combined influences of
319 surface mean temperature and PW. Surface mean temperature rise (fall) will strengthen
320 (weaken) the atmospheric circulation in favor of increased VCWC in the non-monsoon
321 and Tibetan Plateau sub-regions, but weaken (strengthen) the climate systems in the
322 monsoon sub-region. This explains the positive correlation between surface mean
323 temperature and VCWC in the non-monsoon and Tibetan Plateau sub-regions but
324 significantly negative correlation in the monsoon sub-region (Table 2). Meanwhile, PW
325 increases will moderate the regional atmospheric circulation systems in favor of
326 increased VCWC in all of the three sub-regions (Figure 10). On the other hand, surface
327 mean temperature will also influence PW. For example, surface mean temperature
328 increase in the non-monsoon sub-region is conducive to increased evaporation and
329 warmer temperatures will increase the saturation vapor pressure, leading to increased
330 PW.

331 Different rates of local temperature change can influence the temperature gradient
332 between regions, which can in turn influence water vapor transport between these
333 regions. For example, more rapid warming at the surface in the Tibetan Plateau sub-

334 region than further south in the free atmosphere will enhance the plateau heat source
335 effect (the meridional temperature gradient is already reversed in summer), strengthen
336 the South Asian summer monsoon, and result in an increase of water vapor transport to
337 the plateau region. In contrast, more warming in the north of the monsoon sub-region
338 than in the south will decrease the meridional temperature gradient, pressure gradient,
339 and weaken the East Asian summer monsoon, resulting in a decrease of water vapor
340 transport across the monsoon sub-region. Thus warming appears to have contradictory
341 influences on VCWC in the two parts of China. Clarifying the influences of
342 atmospheric circulation on VCWC in China is thus an urgent task.

343 The sole use of ERA-Interim reanalysis is not enough to fully represent VCWC across
344 China and comparisons from multiple reanalyses are necessary to provide more in-
345 depth analysis. There are known discrepancies between ERA-Interim and
346 NCEP/NCAR in depicting precipitation and atmospheric moisture for example [*J Li et*
347 *al.*, 2017a; *P Li et al.*, 2017b; *R Wang et al.*, 2017a; *Z Wang et al.*, 2017b]. Even for
348 satellite retrieval products, cloud properties still suffer from large uncertainties due to
349 the senor ability, retrieval algorithm and sample timing [*Klein et al.*, 2013]. As for
350 reanalyzed or modelled cloud properties, the spatial pattern may be captured by the
351 reanalysis but the temporal trend is still questionable [*Jiang et al.*, 2012; *Klein et al.*,
352 2013; *Stubenrauch et al.*, 2013]. There are other datasets available for the cloud water
353 used in this study, and there have changes among datasets varied with regions and
354 seasons. The multiple satellite observations (MODIS, ISCCP, and CloudSat) and
355 reanalysis data (ERA-Interim and CFSR) are compared for cloud water in a recent study

356 [*Geng*, 2017]. In terms of cloud water content, ERA-Interim shows high consistency
357 with MODIS and CFSR all showed high consistency. Although the distribution of the
358 high and low values of the four datasets is relatively consistent, the correlation
359 coefficient among them is above 0.6, but there are still differences in the specific values
360 of the cloud water path [*Geng*, 2017]. Though the reanalysis provides relative coherent
361 physics between cloud and meteorological fields through its host assimilation model,
362 the model parameterization biases are unavoidable. Thus, it should be cautious to use
363 the reanalyzed cloud properties for climate trend analysis. Furthermore there are also
364 strong seasonal differences in both the intensity and spatial distribution of VCWC, and
365 so an examination beyond the summer is required. Additional work will focus on other
366 seasons and the extent to which other reanalyses corroborate our current findings.
367
368
369 **Acknowledgments.** This study is supported by National Key R&D Program of China
370 (2016YFA0601702), National Natural Science Foundation of China (41771069). This
371 study is also funded by "the Priority Academic Program Development of Jiangsu
372 Higher Education Institutions" (PAPD).
373
374 **References**
375 Bannister, D., M. Herzog, H.-F. Graf, J. S. Hosking, and C. A. Short (2017), An
376 Assessment of Recent and Future Temperature Change over the Sichuan Basin, China,
377 Using CMIP5 Climate Models, *Journal of Climate*, *30*(17), 6701-6722.

Bony, S., et al. (2015), Clouds, circulation and climate sensitivity, *Nature Geoscience*, *8*, 261, doi:10.1038/ngeo2398.

Dee, D. P., and S. Uppala (2009), Variational bias correction of satellite radiance data in the ERA-Interim reanalysis, *Quarterly Journal of the Royal Meteorological Society*, *135*(644), 1830-1841, doi:10.1002/qj.493.

Dee, D. P., et al. (2011), The ERA-Interim reanalysis: configuration and performance of the data assimilation system, *Quarterly Journal of the Royal Meteorological Society*, *137*(656), 553-597, doi:10.1002/qj.828.

Ding, Y. H., G. Y. Ren, Z. C. Zhao, Y. Xu, Y. Luo, Q. P. Li, and J. Zhang (2007), Detection, causes and projection of climate change over China: An overview of recent progress, *Advances in Atmospheric Sciences*, *24*(6), 954-971.

Geng, R. (2017), Comparison and analysis of atmospheric water cycle variables based on satellite and reanalysis data, *Hefei: University of Science and Technology of China (in Chinese)*, 1-52.

Gultepe, I., and G. A. Isaac (1997), Liquid Water Content and Temperature Relationship from Aircraft Observations and Its Applicability to GCMs, *Journal of Climate*, *10*(3), 446-452.

IPCC (2013), Summary for Policymakers of Climate change 2013: The Physical Science Basis. Contribution of Working Group I to the Fifth Assessment Report of the Intergovernmental Panel on Climate Change *Cambridge, UK: Cambridge University Press*.

Jiang, J. H., et al. (2012), Evaluation of cloud and water vapor simulations in CMIP5

climate models using NASA “A-Train” satellite observations, *Journal of Geophysical Research: Atmospheres*, *117*(D14), doi:10.1029/2011JD017237.

Klein, S. A., Y. Zhang, M. D. Zelinka, R. Pincus, J. Boyle, and P. J. Gleckler (2013), Are climate model simulations of clouds improving? An evaluation using the ISCCP simulator, *Journal of Geophysical Research: Atmospheres*, *118*(3), 1329-1342, doi:doi:10.1002/jgrd.50141.

Lanzante, J. R. (1984), A Rotated Eigenanalysis of the Correlation between 700 mb Heights and Sea Surface Temperatures in the Pacific and Atlantic, *Monthly Weather Review*, *112*(11), 2270-2280.

Li, J., W.-C. Wang, X. Dong, and J. Mao (2017a), Cloud-radiation-precipitation associations over the Asian monsoon region: an observational analysis, *Climate Dynamics*, *49*(9), 3237-3255, doi:10.1007/s00382-016-3509-5.

Li, P., T. Zhou, and X. Chen (2017b), Water vapor transport for spring persistent rains over southeastern China based on five reanalysis datasets, *Climate Dynamics*, *in press*.

Li, X., Z. Wen, and W. Zhou (2011), Long-term Change in Summer Water Vapor Transport over South China in Recent Decades, *Journal of the Meteorological Society of Japan*, *89A*, 271-282.

Liu, B. H., M. Xu, M. Henderson, Y. Qi, and Y. Q. Li (2004), Taking China's temperature: Daily range, warming trends, and regional variations, 1955-2000, *Journal of Climate*, *17*(22), 4453-4462.

Norris, J. R., R. J. Allen, A. T. Evan, M. D. Zelinka, C. W. O’Dell, and S. A. Klein (2016), Evidence for climate change in the satellite cloud record, *Nature*, *536*, 72,

422 doi:10.1038/nature18273.
423 Ntwali, D., E. Mugisha, F. Vuguziga, and D. Kakpa (2017), Liquid and ice water content
424 in clouds and their variability with temperature in Africa based on ERA-Interim, JRA-
425 55, MERRA and ISCCP, *Meteorology and Atmospheric Physics*, *129*(1), 17-34,
426 doi:10.1007/s00703-016-0447-z.
427 Overland, J. E., and R. W. Preisendorfer (1982), A Significance Test for Principal
428 Components Applied to a Cyclone Climatology, *Monthly Weather Review*, *110*(1), 1-4.
429 Shen, S., and K. M. Lau (1995), Biennial Oscillation Associated with the East Asian
430 Summer Monsoon and Tropical Sea Surface Temperatures, *Journal of the*
431 *Meteorological Society of Japan. Ser. II*, *73*(1), 105-124.
432 Stubenrauch, C. J., et al. (2013), Assessment of Global Cloud Datasets from Satellites:
433 Project and Database Initiated by the GEWEX Radiation Panel, *Bulletin of the*
434 *American Meteorological Society*, *94*(7), 1031-1049, doi:10.1175/BAMS-D-12-
435 00117.1.
436 Wallace, J. M., C. Smith, and C. S. Bretherton (1992), Singular Value Decomposition
437 of Wintertime Sea Surface Temperature and 500-mb Height Anomalies, *Journal of*
438 *Climate*, *5*(6), 561-576.
439 Wang, H. J., J. Q. Sun, H. P. Chen, Y. L. Zhu, Y. Zhang, D. B. Jiang, X. M. Lang, K.
440 Fan, E. T. Yu, and S. Yang (2012), Extreme Climate in China: Facts, Simulation and
441 Projection, *Meteorologische Zeitschrift*, *21*(3), 279-304, doi:10.1127/0941-
442 2948/2012/0330.
443 Wang, R., Y. Fu, T. Xian, F. Chen, R. Yuan, R. Li, and G. Liu (2017a), Evaluation of

444 Atmospheric Precipitable Water Characteristics and Trends in Mainland China from
445 1995 to 2012, *Journal of Climate*, *30*(21), 8673-8688, doi:10.1175/JCLI-D-16-0433.1.
446 Wang, S. W., and D. Y. Gong (2000), Enhancement of the warming trend in China,
447 *Geophysical Research Letters*, *27*(16), 2581-2584.
448 Wang, Y. Q., and L. Zhou (2005), Observed trends in extreme precipitation events in
449 China during 1961-2001 and the associated changes in large-scale circulation,
450 *Geophysical Research Letters*, *32*(9), L09707.
451 Wang, Z., A. Duan, S. Yang, and K. Ullah (2017b), Atmospheric moisture budget and
452 its regulation on the variability of summer precipitation over the Tibetan Plateau,
453 *Journal of Geophysical Research: Atmospheres*, *122*(2), 614-630,
454 doi:10.1002/2016JD025515.
455 Wu, C., and M. Chou (2013), Tibetan Plateau westerly forcing on the cloud amount
456 over Sichuan Basin and the early Asian summer monsoon, *Journal of Geophysical*
457 *Research: Atmospheres*, *118*(14), 7558-7568, doi:10.1002/jgrd.50580.
458 Wu, H. B., and L. Wu (2005), Methods for diagnosing and forecasting climate
459 variability, *Beijing: China Meteorological Press (in Chinese)*, 113-143.
460 Wu, J., and X. J. Gao (2013), A gridded daily observation dataset over China region
461 and comparison with the other datasets, *Chinese Journal of Geophysics*, *56*(4), 1102-
462 1111.
463 Xu, Y., X. J. Gao, S. Y. Yan, C. H. Xu, Y. Shi, and F. Giorgi (2009), A daily temperature
464 dataset over China and its application in validating a RCM simulation, *Advances in*
465 *Atmospheric Sciences*, *26*(4), 763-772.

466 Yang, D., and P. Wang (2012), Characteristics of Vertical Distributions of Cloud Water
467 Contents over China during Summer, *Chinese Journal of Atmospheric Sciences (in*
468 *Chinese)*, *36*(1), 89-101.
469 Zhai, P., and R. E. Eskridge (1997), Atmospheric Water Vapor over China, *Journal of*
470 *Climate*, *10*(10), 2643-2652.
471 Zhou, T.-J., and R.-C. Yu (2005), Atmospheric water vapor transport associated with
472 typical anomalous summer rainfall patterns in China, *Journal of Geophysical Research:*
473 *Atmospheres*, *110*(D8), D08104, doi:10.1029/2004JD005413.
474
475
476
477
478
479
480
481
482
483
484
485
486
487

Figures

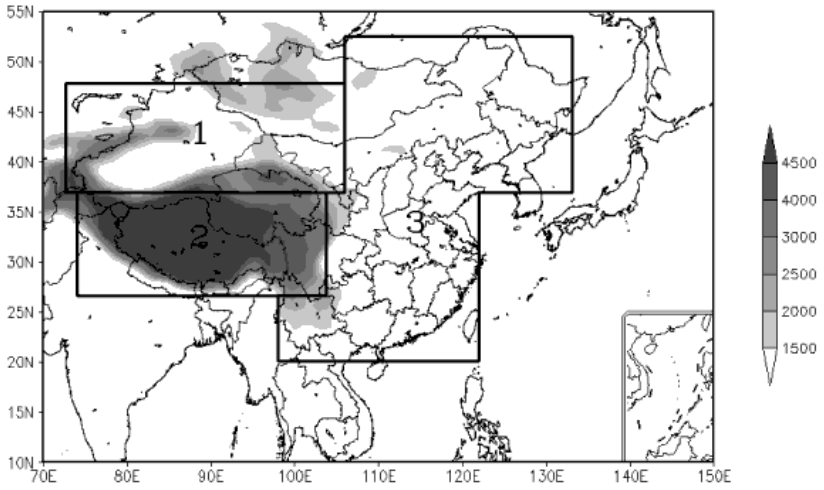

Figure 1. Topographic map of China. The polygons indicate the three sub-regions defined as non-monsoon sub-region (1), Tibetan Plateau sub-region (2) and monsoon sub-region (3).

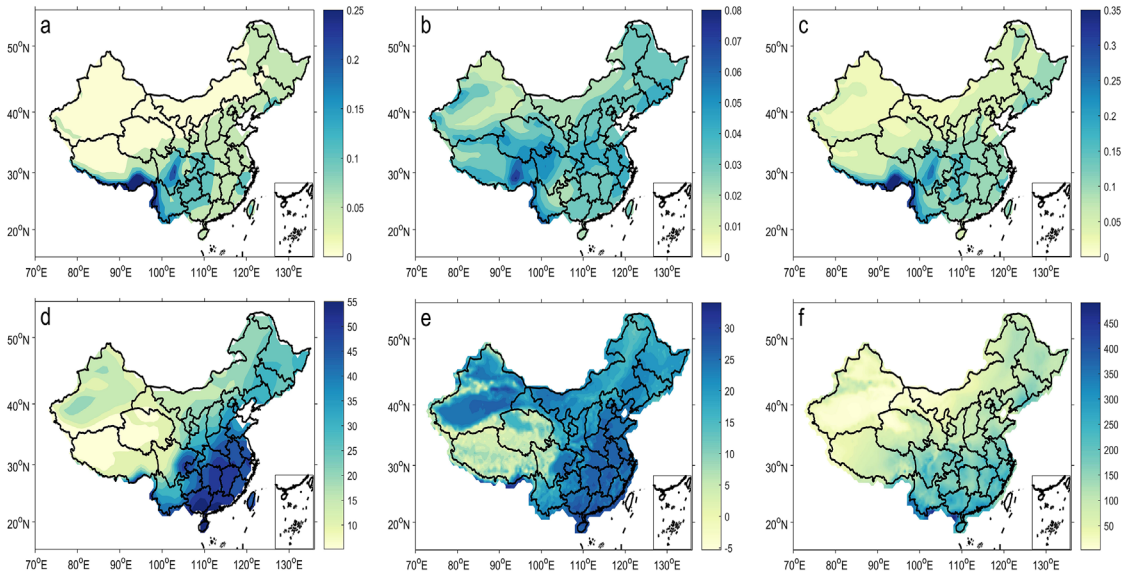

Figure 2. Climatological distribution of vertical integral of a) cloud liquid water content (VCLWC) (kg/m^2), b) cloud ice water content (VCIWC) (kg/m^2), c) cloud water content (VCWC) (kg/m^2), d) precipitable water (PW) (mm), e) surface mean temperature (℃), and f) precipitation (mm) in summer during 1979-2016.

509

510 **Figure 3**. Pressure-latitude cross sections of mean cloud liquid water content (CLWC),
511 cloud ice water content (CIWC) and cloud water content (CWC) across the monsoon
512 sub-region between 106-122°E (panels a,b,c), the non-monsoon sub-region between
513 73-106°E (panels d,e,f), and the Tibetan Plateau sub-region between 74-104°E (panels
514 g,h,i). All units are g/kg, and black dotted lines are isotherms with an interval of 5℃.

515

516

517

518

519

520

Figure 4. Time series of vertical integral of a) cloud liquid water content (kg/m^2), b) cloud ice water content (kg/m^2), c) cloud water content (kg/m^2), d) precipitable water (mm), e) surface mean temperature (℃) and f) precipitation (mm) in the monsoon sub-region (top panel), non-monsoon sub-region (middle panel) and Tibetan Plateau sub-region (bottom panel) in China in summer during 1979-2016. The black curve is a 9 year moving average, and the blue dotted line is the linear trend.

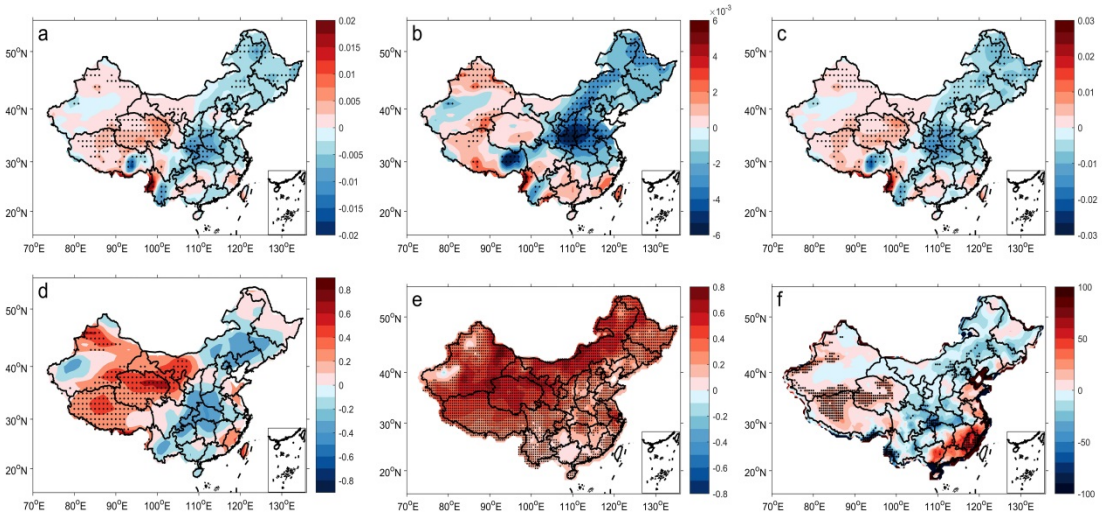

Figure 5. Spatial trends of vertical integral of a) cloud liquid water content (kg/m^2/decade), b) cloud ice water content (kg/m^2/decade), c) cloud water content (kg/m^2/decade), d) precipitable water (mm/decade), e) surface mean temperature (℃/decade), and f) precipitation (mm/decade) in China in summer during 1979-2016. The stippled area indicates significance at the level of 0.05.

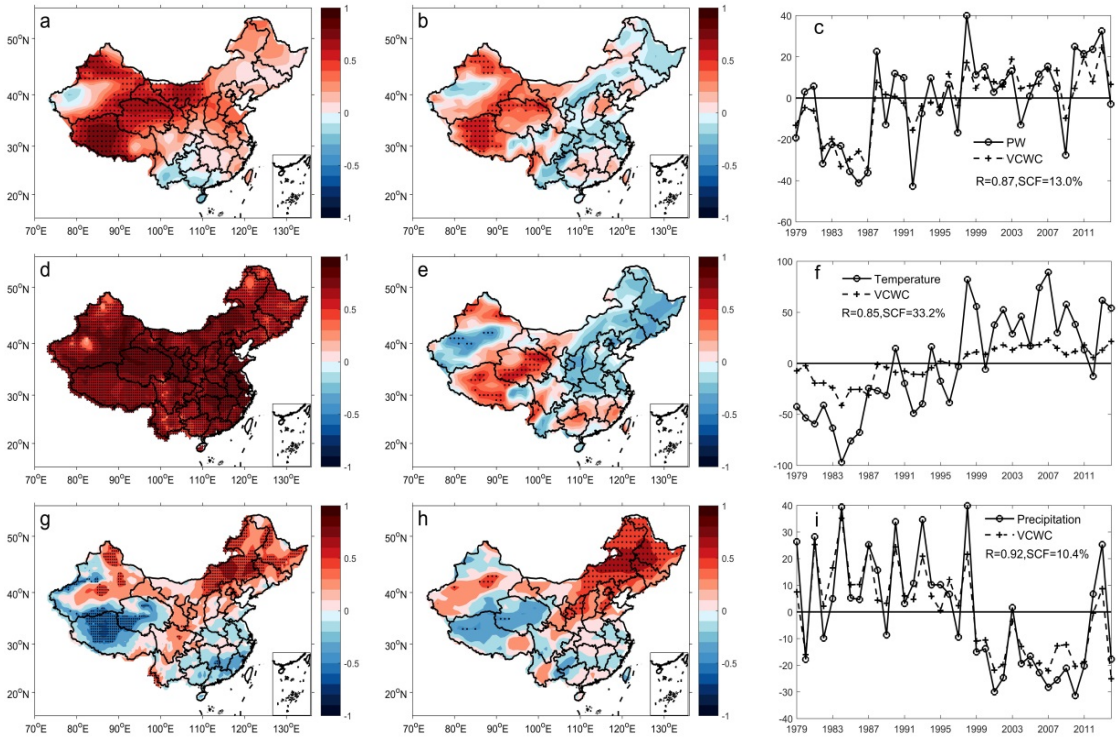

545

546 **Figure 6**. Heterogeneous correlation and time coefficient of the first mode of SVD:

547 panels a-c: precipitable water (PW) and vertical integral of cloud water content

548 (VCWC); panels d-f: surface mean temperature and VCWC; panels g-i: precipitation

549 and VCWC. Stippled areas indicate significance at the level of 0.1. R and SCF indicate

550 the correlation coefficient and squared covariance fraction, respectively.

551

552

553

554

555

556

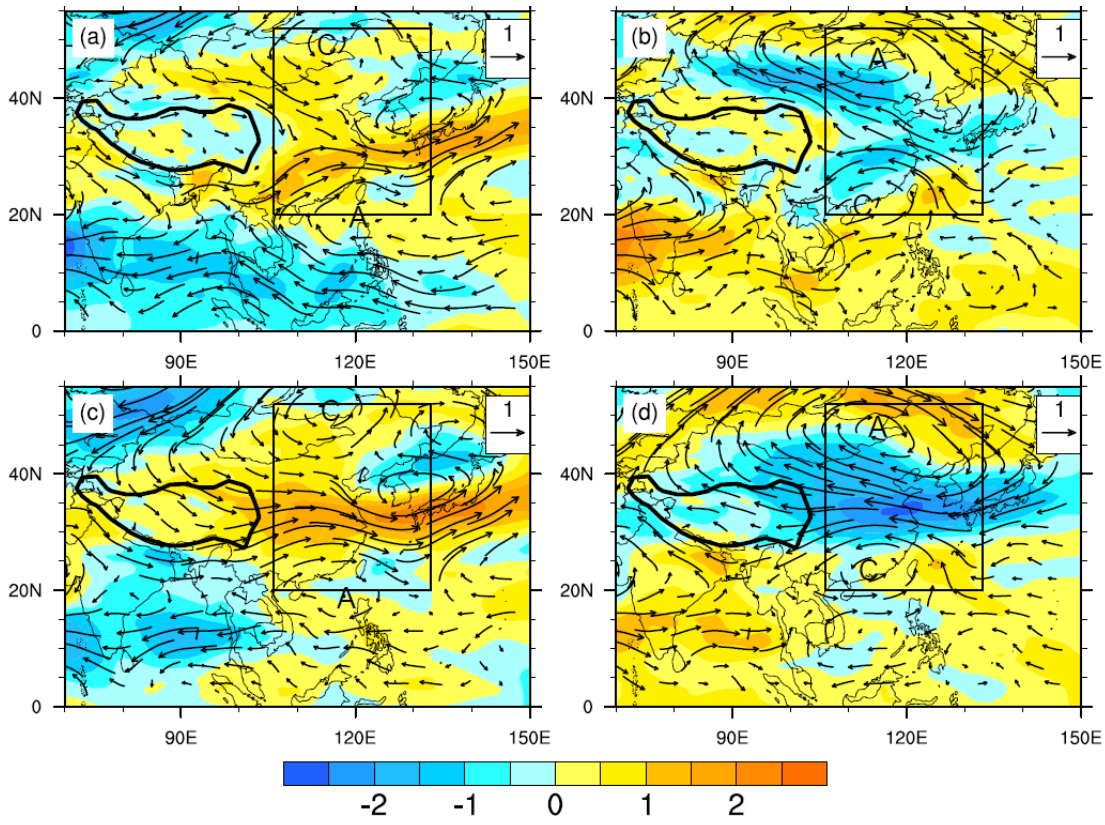

Figure 7. Differences in wind field and wind speed at 700 hPa (top panel a and b) and 500 hPa (bottom panel c and d) between composites of strongly positive and negative mean vertical integral of cloud water content (VCWC, left panel a and c)/surface mean temperature (right panel b and d). Extreme years are defined by deviations exceeding ±0.8σ for the monsoon sub-region (box) during 1979-2016. Strongly positive VCWC years include 1979, 1983, 1993, 1995, 1998, 1999, 2003, and strongly negative VCWC years include 2001, 2006, 2007, 2008, 2009, 2010, 2011, and 2013, respectively. Strongly positive surface mean temperatures occurred in 1994, 1997, 2000, 2001, 2005, 2006, 2007, 2010, 2011, 2013, and strongly negative surface mean temperature occurred in 1979, 1983, 1984, 1986, 1987, 1989, 1992, 1993, 1996, respectively. The anomalous flow is represented by the arrows, and the shaded areas indicate wind speed difference. Positive/negative differences mean enhanced westerly/easterly flow. "A" and "C" represent anticyclonic and cyclonic systems.

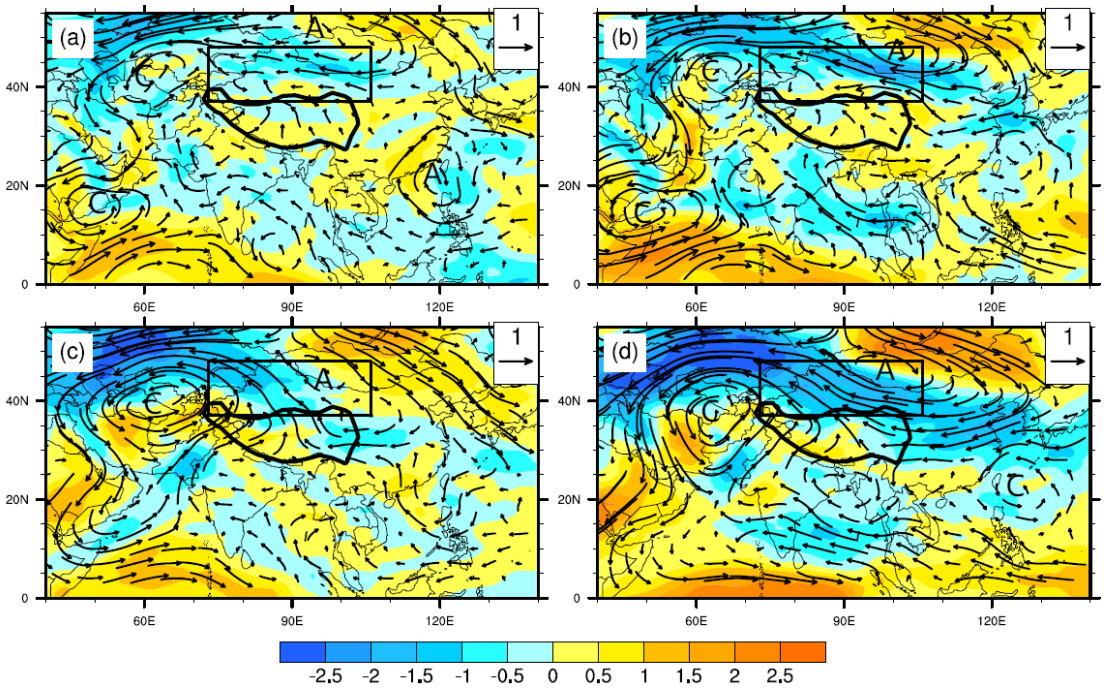

574

575 **Figure 8**. Differences in wind field and wind speed at 700 hPa (top panel a and b) and
576 500 hPa (bottom panel c and d) between composites of strongly positive and negative
577 mean vertical integral of cloud water content (VCWC, left panel a and c)/precipitable
578 water (right panel b and d). Extreme years are defined by deviations exceeding ±0.8σ
579 for the non-monsoon sub-region (box) during 1979-2016. Strongly positive VCWC was
580 recorded in 1981, 1987, 1993, 1996, 2013, 2016, and strongly negative VCWC in 1980,
581 1983, 1984, 1985, 1990, 1995, 2008,2009, respectively. Strongly positive precipitable
582 water was recorded in 1981, 1998, 1999, 2000, 2012, 2016, and strongly negative
583 precipitable water in 1980, 1982, 1984, 1985, 2008, 2009, respectively. . The anomalous
584 flow is represented by the arrows, and the shaded areas indicate wind speed difference.
585 Positive/negative differences mean enhanced westerly/easterly flow. “A” and “C”
586 represent anticyclonic and cyclonic systems. The key is the same as in Figure 7.

587

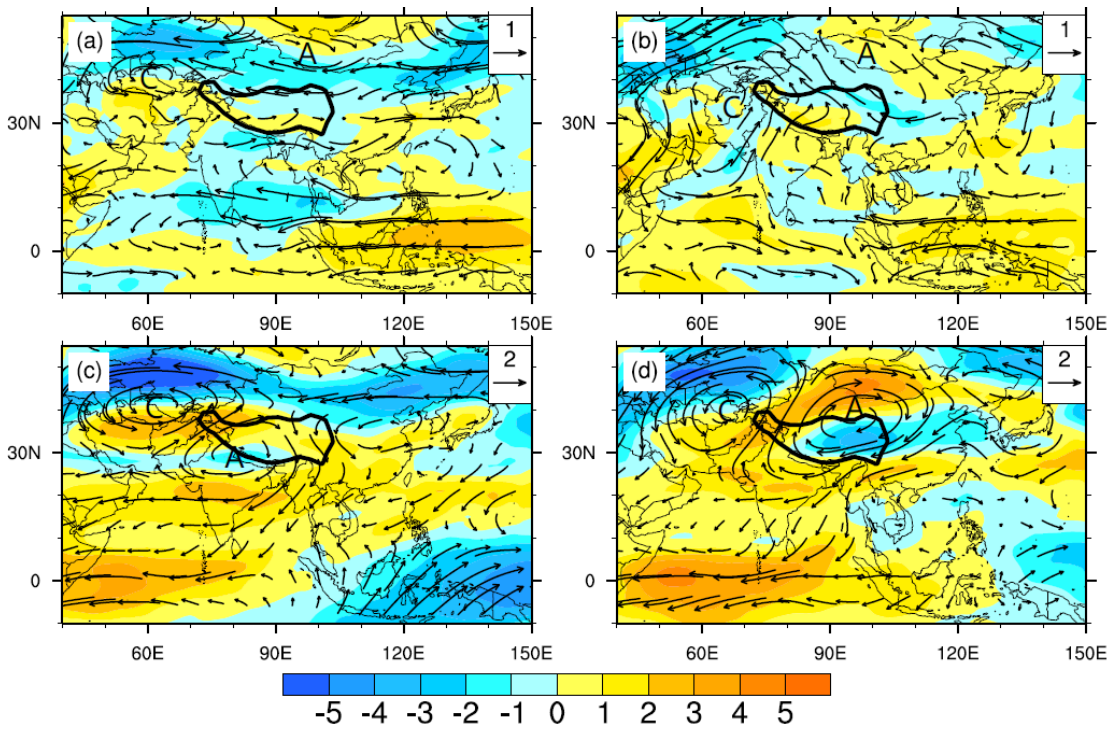

Figure 9. Differences in wind field and wind speed at 500 hPa (top panel a and b) and 200 hPa (bottom panel c and d) between composites of strongly positive and negative mean vertical integral of cloud water content (VCWC, left panel a and c)/surface mean temperature (right panel b and d). Extreme years are defined by deviations exceeding ±0.8σ for the Tibetan plateau sub-region during 1979-2016. Strongly positive VCWC occurred in 1988, 1998, 1999, 2003, 2008, and strongly negative VCWC occurred in 1979,1982, 1983, 1984, 1986, 1992, 1994, 2006, 2009, 2013, respectively. Strongly positive surface mean temperature was recorded in 1998, 2006, 2009, 2010, 2012, 2013, 2014, and strongly negative surface mean temperature in 1979, 1980, 1982, 1983, 1984, 1985, 1986, 1989, 1992, respectively. . The anomalous flow is represented by the arrows, and the shaded areas indicate wind speed difference. Positive/negative differences mean enhanced westerly/easterly flow. “A” and “C” represent anticyclonic and cyclonic systems. The key is the same as in Figure 7.

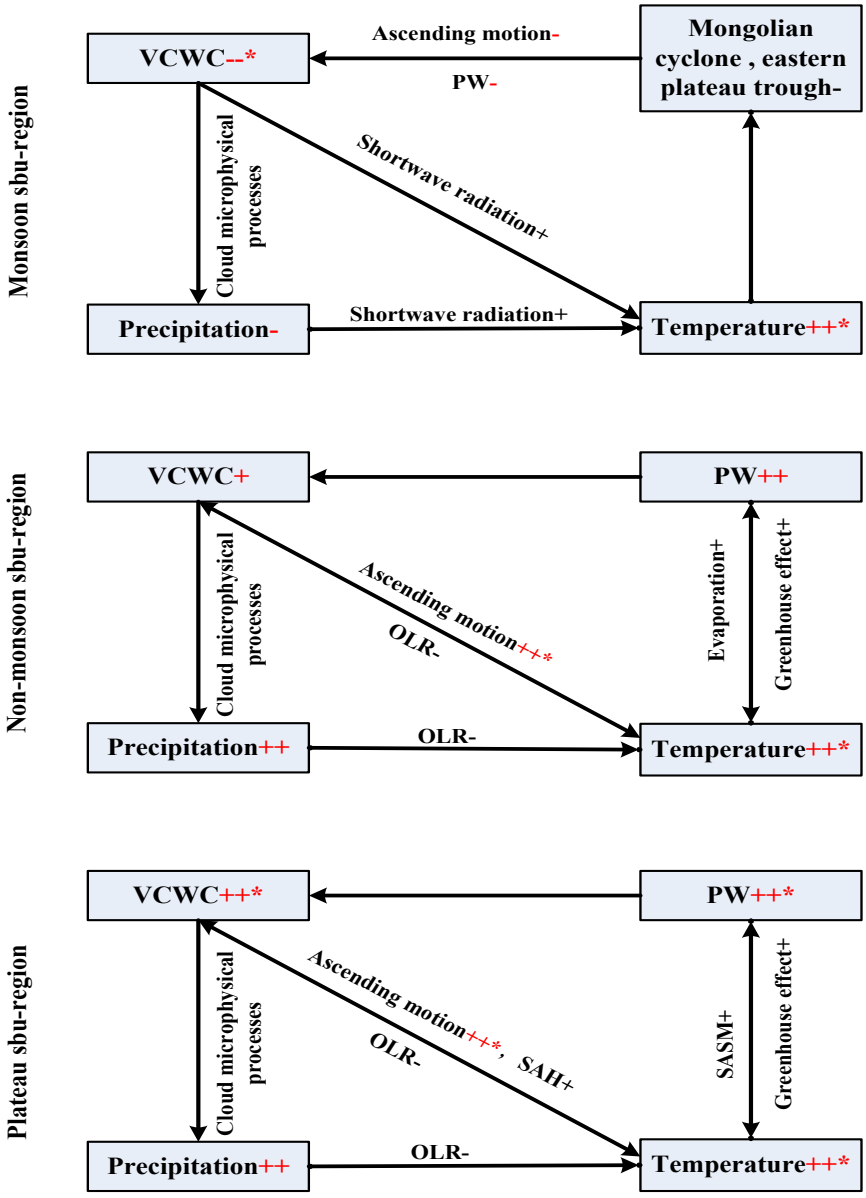

606

607 **Figure 10**. A schematic representation of the climate system which influences summer
608 cloud water content in the three sub-regions of China. SAH, SASM and OLR indicate
609 south Asian high, south Asian monsoon, and outgoing longwave radiation, respectively.
610 The red +/-, ++/--, ++*/--* represent weak increase/decrease, strong increase/decrease,
611 strong increase/decrease which passes significance at the level of 0.05.

612

613

614

615

Tables

Table 1. Trends of vertical integral of cloud water content (VCWC, g/m^2/decade), precipitation (mm/decade), precipitable water (PW, mm/decade) and surface mean temperature (℃/decade) in the non-monsoon sub-region, monsoon sub-region and Tibetan Plateau sub-region during 1979-2016. Values with * and ** indicate significance at the level of 0.05 and 0.01, respectively.

	VCWC	Precipitation	PW	Surface mean temperature
Monsoon sub-region	-2.71*	-0.97	0	0.28**
Non-monsoon sub-region	1.04	3.17	0.19	0.43**
Tibetan Plateau sub-region	3.39*	3.59	0.42**	0.41**

646 **Table 2**. Correlations between vertical integral of cloud water content (VCWC), cloud
647 liquid water content (VCLWC), cloud ice water content (VCIWC), precipitation,
648 precipitable water (PW) and surface mean temperature in the non-monsoon sub-region,
649 monsoon sub-region and Tibetan Plateau sub-region during 1979-2016. Value with *
650 and ** indicate significance at the level of 0.05 and 0.01, respectively.

	Monsoon sub-region			Non-monsoon sub-region			Tibetan Plateau sub-region		
	VCWC	VCLWC	VCIWC	VCWC	VCLWC	VCIWC	VCWC	VCLWC	VCIWC
Precipitation	0.51**	0.48**	0.51**	0.73**	0.67**	0.65**	0.44**	0.44**	0.36*
Surface mean temperature	-0.51**	-0.55**	-0.40*	-0.05	-0.08	0	0.31	0.40*	0.02
PW	0.18	0.18	0.15	0.78**	0.86**	0.50**	0.68**	0.73**	0.41**

651